Jour. Ind. Inst. Sc. 61 (A), Sept. 1979, pp. 175-194

The truncated dielectric-coated conducting sphere—radiation and gain characteristics

PARVEEN WAHID AND R. CHATTERJEE
Department of Electrical Communication Engineering, Indian Institute of Science, Bangalore 560 012.

Received on July 3, 1979.

Abstract

An exhaustive study of the radiation and gain characteristics of a truncated dielectric-coated conducting spherical antenna excited in the symmetric TM mode has been reported. The effect of the various structure parameters on the radiation and the gain characteristics for a few even and odd order TM_{on} modes for different structures is shown. The theoretical radiation patterns and gain have been compared with experiment. It is found that there is good agreement between theory and experiment in the case of TM_{05} and TM_{06} modes. A theoretical and experimental study of the radiation and gain characteristics in the frequency range 8·0 to 12·0 GHz has been reported.

Key words : Dielectric-coated antennas, radiation and gain characteristics.

1. Introduction

Significant contributions in the field of dielectric-coated antennas have been made in the recent years. Investigations on dielectric-coated cylindrical antennas have been reported by Ting[1] and Chatterjee *et al*[2, 3]. An extensive theoretical and experimental study of dielectric-coated conducting conical antennas has been carried out by Chatterjee *et al*[4, 5]. Yeh[6] has studied the dielectric-coated prolate spheroid as an antenna and Neelakantaswamy[7] has reported work done on conducting corrugated spherical antennas. An approximate treatment of the dielectric-coated conducting spherical antenna excited in the hybrid mode and the symmetric TM mode has been reported by Chatterjee *et al*[8, 9].

In the present paper, an exhaustive study of the radiation and gain characteristics of a truncated dielectric-coated conducting spherical antenna excited in the symmetric TM mode has been done. This is an extension of the work reported earlier[10]. A number of even and odd order TM_{on} modes have been studied. The effect of various structure parameters on the radiation characteristics has been reported. The theoretical results obtained have been verified experimentally.

2. Radiation field of the truncated dielectric-coated conducting spherical antenna

Figure 1 is a photograph of the truncated dielectric-coated conducting spherical antennas. The structure has been excited in the symmetric transverse magnetic mode by a coaxial line[11]. Such a structure can be assumed to be excited by a delta-function electric field source $E_0 e^{-j\omega t}$ applied normally over an annular ring of radius $b \sin \theta_1$ and width $(b - a) \sin \theta_1$; θ_1 being the angle of excitation. The near-field components E_r, E_θ and H_ϕ are given by[12]

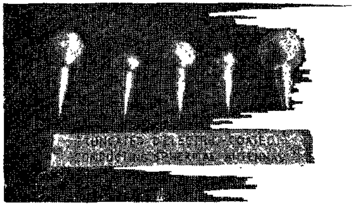

FIG. 1. Truncated dielectric-coated conducting spherical antennas.

Region I : $a \leqslant r \leqslant b$

$$E_r^i = -\sum_n \frac{n(n+1)}{k_1 r} P_n(\cos\theta)\,[L_{on} j_n(k_1 r) + M_{on} y_n(k_1 r)]\, e^{-j\omega t} + E_{r_0} \tag{1}$$

$$E_\theta^i = -\sum_n P_n'(\cos\theta)\,[L_{on}[k_1 r j_n(k_1 r)]' + M_{on}[k_1 r y_n(k_1 r)]']\, e^{-j\omega t} + E_{\theta_0} \tag{2}$$

$$H_\phi^i = \frac{k_1}{j\omega\mu_1} \sum_n P_n'(\cos\theta)\,[L_{on} j_n(k_1 r) + M_{on} y_n(k_1 r)] e^{-j\omega t} \tag{3}$$

Region II : $r \geqslant b$

$$E_r^e = -\sum_n n(n+1) P_n(\cos\theta)\, N_{on} \frac{h_n^{(1)}(k_0 r)}{k_0 r} e^{-j\omega t} \tag{4}$$

$$E_\theta^e = -\sum_n P_n'(\cos\theta) \frac{1}{k_0 r} N_{on} [k_0 r\, h_n^{(1)}(k_0 r)]' e^{-j\omega t} \tag{5}$$

$$H_\phi^e = \frac{k_0}{j\omega\mu_0} \sum_n P_n'(\cos\theta)\, N_{on} \frac{1}{k_0 r} h_n^{(1)}(k_0 r)\, e^{-j\omega t} \tag{6}$$

where

$$k_1 = \omega\sqrt{\mu_1\left(\epsilon_1 + j\frac{\sigma_1}{\omega}\right)}\,;\; k_0 = \omega\sqrt{\mu_0\left(\epsilon_0 + j\frac{\sigma_0}{\omega}\right)}\,;$$

ϵ_1, μ_1, σ_1 and ϵ_2, μ_2, σ_2 are the characteristics of medium I and II respectively; ω is the angular frequency; $P_n(\cos\theta)$ is the Legendre function; $j_n(k_1 r)$, $y_n(k_1 r)$ and $h_n^{(1)}(k_0 r)$ are the spherical Bessel, Neumann and Hankel function of the first kind respectively ; L_{on}, M_{on} and N_{on} are the amplitude coefficients. a and b are the inner and outer radius respectively of the dielectric-coated conducting sphere.

2.1. *Application of Love-Schelkunoff's equivalence principle*

Knowing the field components inside and outside the dielectric-coated conducting sphere the radiation field can be determined by using Love–Schelkunoff's equivalence principle. This principle can be stated mathematically as

$$\vec{J} = \vec{n} \times \vec{H} ; \quad \vec{M} = -\vec{n} \times \vec{E} \tag{7}$$

where $\vec{n}$ is the outward drawn normal to the surface S, $\vec{E}$ and $\vec{H}$ are the electric and magnetic field vectors on the surface S; $\vec{J}$ and $\vec{M}$ are the surface electric and magnetic current densities, respectively. The surface S is selected as a closed surface consisting of the surface S_1 of the truncated dielectric-coated conducting sphere, the outer surface S_2 of the mode transducer and an infinitely large sphere S_3 to close it as shown in Fig. 2. The only currents of importance on this surface are the electric and magnetic currents on the surface S_1, assuming the currents on the surfaces S_2 and S_3 are negligible.

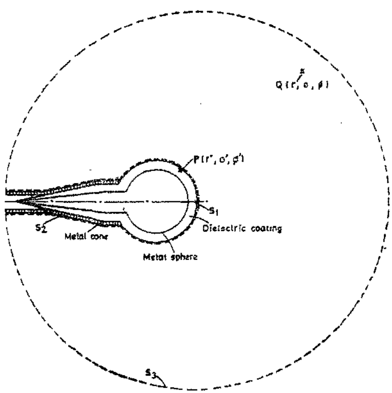

FIG. 2. Surface S used in the application of Love-Schelkunoff's equivalence principle $S = S_1 + S_2 + S_3$.

2.2. *Radiation vectors*

The radiation fields at a distant point (r, θ, ϕ) are given by

$$E_\theta = \eta H_\phi = -\frac{j}{2\lambda_0 r}[\eta_0 L_\theta^m + L_\phi^e] \tag{8}$$

$$E_\phi = -\eta H_\theta = -\frac{j}{2\lambda_0 r}[\eta_0 L_\phi^m + L_\theta^e] \tag{9}$$

where λ_0 is the free space wave-length corresponding to the frequency of excitation, η_0 is the characteristic impedance of free space, $\vec{L}^e$ and $\vec{L}^m$ are the electric radiation vector and magnetic radiation vector respectively. $\vec{L}^e$ and $\vec{L}^m$ are expressed as

$$\vec{L}^e = \int_{\text{space}} e^{j\beta_0 PQ}\, \vec{dp}^m\, e^{-j\omega t} \tag{10}$$

$$\vec{L}^m = \int_{\text{space}} e^{j\beta_0 PQ}\, \vec{dp}^e\, e^{-j\omega t} \tag{11}$$

where $\beta_0 = k_0 = 2\pi/\lambda_0 = \omega\sqrt{\mu_0\epsilon_0}$ outside the sphere, $\vec{dp}^e$ and $\vec{dp}^m$ are the moments of the electric and magnetic current elements situated at the source point $P(r', \theta', \phi')$ and are expressed as

$$\vec{dp}^e = (\vec{n} \times \vec{H})\, ds \tag{12}$$

$$\vec{dp}^m = -(\vec{n} \times \vec{E})\, ds \tag{13}$$

ds is an elementary area on the surface of the truncated dielectric-coated conducting sphere $= b^2 \sin\theta\, d\theta\, d\phi$. PQ is the distance between the source point $P(r', \theta', \phi')$ and the distant point $Q(r, \theta, \phi)$.

$$\begin{aligned} PQ &= r - r'\cos\theta\cos\theta' - r'\sin\theta\sin\theta'\cos(\phi - \phi') \\ &= r - b\cos\theta\cos\theta' - b\sin\theta\sin\theta'\cos(\phi - \phi') \end{aligned} \tag{14}$$

since $r' = b$ on the surface of the truncated dielectric-coated conducting sphere.

The electric and magnetic current densities (eqn. 7) are given by

$$\vec{J} = \vec{n} \times \vec{H} = -\vec{\theta} H_\phi \tag{15}$$

$$\vec{M} = -\vec{n} \times \vec{E} = -\vec{\phi} E_\theta. \tag{16}$$

Therefore eqns. (12) and (13) become

$$\vec{dp}^e = -\vec{\theta} H_{\phi'}\, ds \tag{17}$$

$$\vec{dp}^m = -\vec{\phi} E_{\theta'}\ ds \tag{18}$$

$E_{\phi'}$ and $H_{\theta'}$ being the magnetic and electric field components on the surface of the dielectric-coated conducting sphere, given by eqns. (5) and (6). Substituting eqns. (17) and (18) in eqns. (10) and (11), we get

$$\vec{L}^e = -\int_{\theta'=0}^{\theta_1} \int_{\phi'=0}^{2\pi} \exp [jk_0 [r - b\cos\theta\cos\theta'$$
$$- b\sin\theta\sin\theta'\cos(\phi - \phi')]] \vec{\phi'} E_{\theta'} \exp(-j\omega t)\, b^2 \sin\theta'\, d\theta'\, d\phi' \tag{19}$$

$$\vec{L}^m = -\int_{\theta'=0}^{\theta_1} \int_{\phi'=0}^{2\pi} \exp [jk_0 [r - b\cos\theta\cos\theta'$$
$$- b\sin\theta\sin\theta'\cos(\phi - \phi')]] \vec{\theta'} H_{\phi'} \exp(-j\omega t)\, b^2 \sin\theta'\, d\theta'\, d\phi'. \tag{20}$$

A transformation to rectangular coordinates gives

$$L_x^e = -L_{\phi'}^e \sin\phi', \quad L_y^e = L_{\phi'}^e \cos\varphi', \quad L_z^e = 0$$

$$L_x^m = L_{\theta'}^m \cos\theta'\cos\phi', \quad L_y^m = L_{\theta'}^m \cos\theta'\sin\phi', \quad L_z^m = -L_{\theta'}^m \sin\theta'.$$

Therefore on transformation, we get

$$L_x^e = -2\pi j b^2 \sin\phi \exp[j(k_0 r - \omega t)] \int_{\theta'=0}^{\theta_1} J_1(k_0 b\sin\theta\sin\theta')$$
$$\times \exp(-jk_0 b\cos\theta\cos\theta')\ E_{\theta'} \sin\theta'\, d\theta' \tag{21}$$

$$L_y^e = 2\pi j b^2 \cos\phi \exp[j(k_0 r - \omega t)] \int_{\theta'=0}^{\theta_1} J_1(k_0 b\sin\theta\sin\theta')$$
$$\times \exp(-jk_0 b\cos\theta\cos\theta')\, E_{\theta'} \sin\theta'\, d\theta' \tag{22}$$

$$L_z^e = 0 \tag{23}$$

$$L_x^m = 2\pi j b^2 \cos\phi \exp[j(k_0 r - \omega t)] \int_{\theta'=0}^{\theta_1} J_1(k_0 b\sin\theta\sin\theta')$$
$$\times \exp(jk_0 b\cos\theta\cos\theta')\, H_{\phi'} \cos\theta'\sin\theta'\, \mathrm{d}\theta' \tag{24}$$

$$L_y^m = 2\pi j b^2 \sin\phi \exp[j(k_0 r - \omega t)] \int_{\theta'=0}^{\theta_1} J_1(k_0 b\sin\theta\sin\theta')$$
$$\times \exp(-jk_0 b\cos\theta\cos\theta')\, H_{\phi'} \sin\theta'\cos\theta'\, d\theta' \tag{25}$$

$$L_z^m = 2\pi b^2 \exp[j(k_0 r - \omega t)] \int_{\theta'=0}^{\theta_1} J_0(k_0 b\sin\theta\sin\theta')$$
$$\times \exp(jk_0 b\cos\theta\cos\theta')\, H_{\phi}' \sin^2\theta'\, \mathrm{d}\theta'. \tag{26}$$

At the distant point Q we have

$$L_\theta^e = \cos\theta\cos\phi\, L_x^e + \cos\theta\sin\phi\, L_y^e - \sin\theta\, L_z^e$$

$$L_\theta^m = \cos\theta\cos\phi\, L_x^m + \cos\theta\sin\phi\, L_y^m - \sin\theta\, L_z^m$$

$$L_\phi^e = -\sin\phi\, L_x^e + \cos\phi\, L_y^e$$

$$L_\phi^m = -\sin\phi\, L_x^m + \cos\phi\, L_y^m.$$

Therefore, we have on simplification

$$L_\theta^e = 0 \tag{27}$$

$$L_\phi^e = 2\pi j b^2 \exp[j(k_0 r - \omega t)] \int_{\theta'=0}^{\theta_1} J_1(k_0 b \sin\theta\sin\theta') \times \exp(-jk_0 b\cos\theta\cos\theta')\, E_{\theta'} \sin\theta'\, d\theta' \tag{28}$$

$$\begin{aligned} L_\theta^m = {} & 2\pi j b^2 \cos\theta \exp[j(k_0 r - \omega t)] \int_{\theta'=0}^{\theta_1} J_1(k_0 b\sin\theta\sin\theta') \\ & \times \exp(-jk_0 b\cos\theta\cos\theta')\, H_{\phi'} \cos\theta' \sin\theta'\, d\theta' \\ & - 2\pi b^2 \sin\theta \exp[(j(k_0 r - \omega t)] \int_{\theta'=0}^{\theta_1} J_0(k_0 b\sin\theta\sin\theta') \\ & \times \exp(-jk_0 b\cos\theta\cos\theta')\, H_{\phi'} \sin^2\theta'\, d\theta' \end{aligned} \tag{29}$$

$$L_\phi^m = 0. \tag{30}$$

Substituting for $E_{\theta'}$ and $H_{\phi'}$ from eqns. (5) and (6) in eqns. (28) and (29), we have

$$\begin{aligned} L_\phi^e = {} & 2\pi j b^2 N_{on} \frac{[k_0 b\, h_n^{(1)}(k_0 b)]'}{k_0 b} \exp[j(k_0 r - \omega t)] \\ & \times \int_{\theta'=0}^{\theta_1} J_1(k_0 b\sin\theta\sin\theta') \exp(-jk_0 b\cos\theta\cos\theta') \\ & \times P_n'(\cos\theta') \sin\theta'\, d\theta' \end{aligned} \tag{31}$$

$$\begin{aligned} L_\theta^m = {} & 2\pi b^2 N_{on} \frac{k_0}{j\omega\mu_0} h_n^{(1)}(k_0 b) \exp[j(k_0 r - \omega t)] \\ & \times [j \cos\theta \int_{\theta'=0}^{\theta_1} J_1(k_0 b\sin\theta\sin\theta') \exp(-jk_0 b\cos\theta\cos\theta') \\ & \times P_n'(\cos\theta') \cos\theta' \sin\theta'\, d\theta' - \sin\theta \int_{\theta'=0}^{\theta_1} J_0(k_0 b\sin\theta\sin\theta') \\ & \times \exp(-jk_0 b\cos\theta\cos\theta')\, P_n'(\cos\theta') \sin^2\theta'\, d\theta']. \end{aligned} \tag{32}$$

2.3. *Radiation field*

Substituting in eqns. (8) and (9), we have the expression for the radiation field.

$$E_\phi = -\eta H_\theta = -\frac{j}{2\lambda_0 r}(\eta_0 L_\phi^m - L_\theta^e) = 0 \tag{33}$$

$$\begin{aligned}
E_\theta &= \eta H_\phi = -\frac{j}{2\lambda_0 r}(\eta_0 L_\theta^m + L_\phi^e) \\
&= -\frac{j}{2\lambda_0 r}\Big[2\pi b^2 \eta_0 \frac{k_0}{j\omega\mu_0} N_{on} h_n^{(1)}(k_0 b) \\
&\times \exp[j(k_0 r - \omega t)][j\cos\theta \int_{\theta'=0}^{\theta_1} J_1(k_0 b \sin\theta \sin\theta') \\
&\times \exp(-jk_0 b\cos\theta\cos\theta') P_n'(\cos\theta')\cos\theta' \sin\theta' \, d\theta' \\
&- \sin\theta \int_{\theta'=0}^{\theta_1} J_0(k_0 b\sin\theta\sin\theta')\exp(-jk_0 b\cos\theta\cos\theta') \\
&\times P_n'(\cos\theta')\sin^2\theta' \, d\theta'] + 2\pi j b^2 N_{on}\frac{[k_0 b h_n^{(1)}(k_0 b)]'}{k_0 b} \\
&\times \exp[j(k_0 r - \omega t)] \int_{\theta'=0}^{\theta'} J_1(k_0 b\sin\theta\sin\theta') \\
&\times \exp(-jk_0 b\cos\theta\cos\theta') P_n'(\cos\theta')\sin\theta' \, d\theta'\Big].
\end{aligned} \tag{34}$$

The radiation pattern in the plane $\phi = 0°$ is given by eqn. (34) itself since this equation is independent of ϕ.

In the above expression N_{on} is the external amplitude coefficient of the dielectric-coated conducting sphere, a and b are the inner and outer radii respectively, J_0 and J_1 are the Bessel functions of order zero and one respectively.

3. Gain of the antenna

The expression for the gain is

$$\text{Gain} = \frac{r^2 \, |E_\theta|^2_{\max}/\eta_0}{W_R/4\pi}$$

where $|E_\theta|$ is the radiation field given by eqn. (34), η_0 is the intrinsic impedance of free space $= 377\Omega$ and W_R is the total power radiated given by

$$W_R = \frac{\pi}{\eta_0} r^2 \int_{\theta=0}^{\pi} |E_\theta|^2 \sin\theta \, d\theta, \tag{35}$$

Therefore the expression for the gain is

$$\text{Gain} = \frac{4\pi r^2 \,|\, E_\theta \,|^2_{max}/\eta_0}{\dfrac{\pi r^2}{\eta_0} \displaystyle\int_{\theta=0}^{\pi} |\, E_\theta \,|^2 \sin\theta \, d\theta}. \tag{36}$$

4. Numerical computation

The radiation and gain characteristics of the antenna have been computed numerically for different structures for few TM_{on} modes using eqns. (34) and (36).

A theoretical study of the radiation characteristics has been made (i) for different values of a varied from 1·0 to 4·0 cm for fixed values of $(b - a)$ and θ_1, (ii) as a function of $(b - a)$ varied from 0·02 to 0·2 cm for fixed values of a and θ_1, (iii) as a function of θ_1 for θ_1 varying from 100° to 160° for various truncated dielectric-coated conducting spherical antennas. The computations have been carried out for the excitation frequency $= 9·375$ GHz and for a value of ϵ_r, the relative permittivity of the coating material $=$ 2·56. In all cases the first six modes have been considered. Some cases of equatorial excitation have been studied taking the odd order TM_{01}, TM_{03} and TM_{05} modes into consideration. The frequency dependance of the radiation characteristics has been studied for frequencies in the range 8·0 to 12·0 GHz.

5. Analysis

5.1. *Radiation patterns*

The theoretical analysis leads to the following conclusions:

(1) The radiation pattern of the truncated dielectric-coated conducting spherical antenna excited in the symmetric TM mode is characterized by a null in the forward direction ($\theta = 0°$) and two main lobes situated symmetrically with respect to the axis of the antenna and a few side lobes for the case of the odd and even order TM_{on} modes. The theoretical radiation patterns at different frequencies are shown in Fig. 11.

(2) Position of main lobe :

(i) For fixed values of a, b and θ_1 for a particular frequency of excitation, the main lobe shifts towards the axis as the order of the mode increases (Table I).

(ii) As a increases, the main lobe shifts towards the axis (Fig. 3).

(iii) The main lobe position shows only a slight variation with coating thickness for any particular mode considered when all other parameters are held constant (Fig. 3).

(iv) With all the other parameters remaining constant the main lobe shifts towards the axis with increasing values of a for the TM_{06} mode. For the TM_{05} mode it is seen

Table I

Radiation characteristics of the truncated dielectric-coated conducting spherical antenna (Theoretical)

$a = 2\cdot5$ cm, $b = 2\cdot6$ cm, $\theta_1 = 140°$, $f = 9\cdot375$ GHz, $\epsilon_r = 2\cdot56$.

Mode	TM_{01}	TM_{02}	TM_{03}	TM_{04}	TM_{05}	TM_{06}
Position of the main lobe (degrees)	97	135	149	157	23	18
Beam width (degrees)	61	39	29	24	27	20
No. of side lobes	..	1	2	3	3	4

that the main lobe shifts towards the axis up to a certain value of a and then moves away. For the TM_{01}, TM_{02}, TM_{03} and TM_{04} modes, the main lobe is further away from the axis and shows a different variation with a for each mode (Fig. 5).

(v) The position of the main lobe is affected considerably by the angle of excitation θ_1, the other parameters being held constant (Fig. 7).

(vi) As the frequency of excitation is increased keeping the other parameters constant, the main lobe shifts towards the axis for a particular mode (Table II).

(3) Beam width of the main lobe :

(i) For fixed values of a, b and θ_1 for a particular frequency of excitation, the beam width decreases as the order of the mode increases (Table I).

Table II

Frequency dependence of the radiation characteristics (Theoretical)

$a = 3\cdot0$ cm, $b = 3\cdot25$ cm, $\theta_1 = 156\cdot9°$, $\epsilon_r = 2\cdot56$, Mode : TM_{05}.

Frequency (GHz)	8·0	9·0	10·0	11·0	12·0
Position of the main lobe (degrees)	18	17	17	16	15
Beam width (degrees)	18·5	18·0	17·0	16·5	15·5
No. of side lobes	4	4	4	4	4

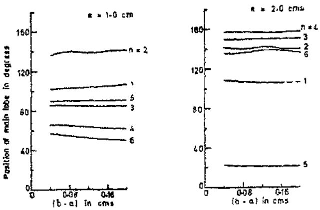

FIG. 3. Variation of the position of the main lobe with coating thickness. $f = 9\cdot375$ GHz, $\varepsilon_r = 2\cdot56$, $\theta_1 = 130°$.

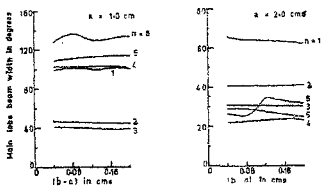

FIG. 4. Variation of main lobe beam width with coating thickness. $f = 9\cdot375$ GHz, $\varepsilon_r = 2\cdot56$, $\theta_1 = 130°$.

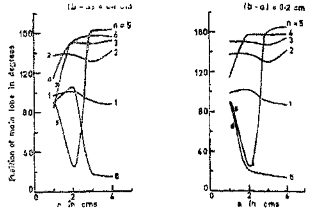

FIG. 5. Variation of the position of the main lobe with the inner radius 'a'. $f = 9\cdot375$ GHz, $\varepsilon_r = 2\cdot56$, $\theta_1 = 130°$.

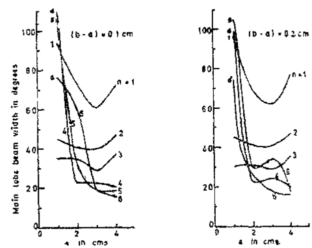

FIG. 6. Variation of the main lobe beam width with the inner radius 'a'. $f = 9\cdot375$ GHz, $\varepsilon_r = 2\cdot56$, $\theta_1 = 130°$.

(ii) The beam width decreases as a increases (Fig. 3).

(iii) The half power beam width shows only a slight variation with coating thickness for any particular mode when all the other parameters are kept constant (Fig. 4).

(iv) The half power beam width shows a variation with a which is different for each mode when all other parameters are maintained constant. For the TM_{01}, TM_{02}, TM_{03} and TM_{04} modes the beam width is minimum for a certain value of a different in each case. For the TM_{05} and TM_{06} modes, it is minimum for the largest value of a considered (Fig. 6).

(v) The beam width shows a variation with the angle of excitation θ_1 for fixed values of a, $(b - a)$ and the frequency of excitation (Fig. 8).

(vi) The main lobe beam width decreases with increase in the frequency of excitation for any particular mode (Table II).

The variation of the position of the main lobe with coating thickness for the case of equatorial excitation is shown in Fig. 9 for the TM_{01}, TM_{03} and TM_{05} modes. For all these modes only a slight variation with coating thickness is seen.

For the TM_{01}, TM_{03} and TM_{05} modes in the case of equatorial excitation, the beam width shows only a slight variation with coating thickness (Fig. 10).

(4) Side lobes :

A theoretical study of the number, position and relative intensity of the side lobes has been made for the antenna and the results are presented in Table A (see Appendix).

(i) The number of side lobes increases with increase in a for the antenna for any particular mode (Table A—Appendix).

(ii) The total number of side lobes increases with increase in the order of the mode *for any particular antenna (Table I).*

(iii) For any particular mode, the number of side lobes tends to remain constant with increase in the frequency of excitation (Table II).

From the theoretical analysis it can be concluded that the radiation characteristics are affected by the structure parameters to varying extents.

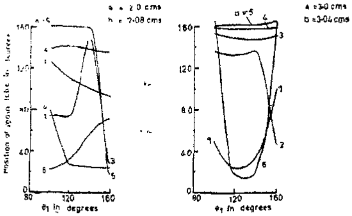

FIG. 7. Variation of the position of the main lobe with θ_1. f = 9·375 GHz, ε_r = 2·56.

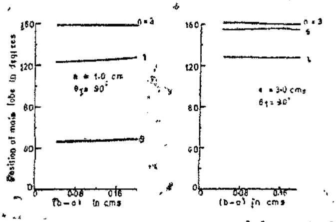

FIG. 9. Variation of the position of the main lobe with coating thickness for equatorial excitation. f = 9·375 GHz, ε_r = 2·56.

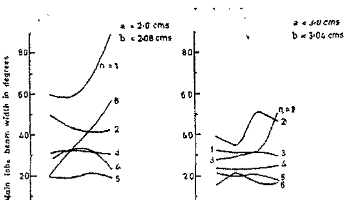

FIG. 8. Variation of main lobe beam width with θ_1. f= 9·375 GHz, ε_r = 2·56.

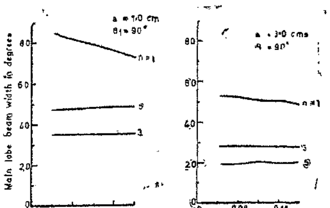

FIG. 10. Variation of the main lobe beam width with coating thickness for equatorial excitation. f = 9·375 GHz, ε_r = 2·56.

5.2. *Gain characteristics*

The theoretical analysis of the gain characteristics leads to the following conclusions:

(i) The gain of the antenna shows a variation with coating thickness for each mode and has a maximum for different values of the coating thickness for each mode in all the cases studied (Fig. 12).

(ii) The angle of excitation θ_1 affects the gain considerably and the variation is different for each mode for fixed values of a, b and the frequency of excitation (Fig. 13).

(iii) The gain varies with the value of the inner radius a going through maximum and minimum values at different values of a for each mode, when $(b - a)$ and θ_1 are kept constant (Fig. 14).

(iv) The value of the gain varies considerably for each individual mode with ϵ_r the relative permittivity of the coating mate ial when the other parameters are kept constant (Fig. 15).

(v) The gain is found to vary with the frequency of excitation for fixed values of a, b and θ_1. The variation is different for each mode for all the cases studied (Fig. 16).

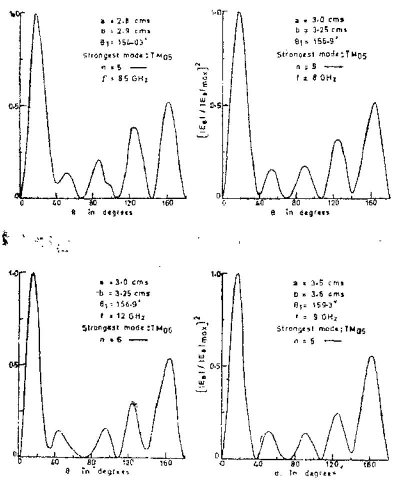

FIG. 11. Normalized radiation patterns at different frequencies for different structures (Theoretical). $\varepsilon_r = 2{\cdot}56$.

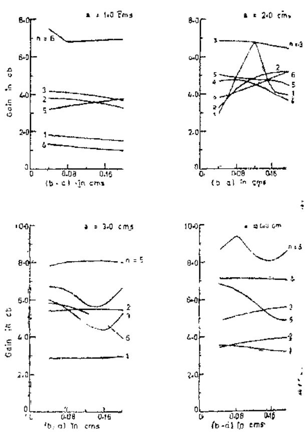

FIG. 12. Variation of gain with coating thickness. f = 9·375 GHz, $\varepsilon_r = 2{\cdot}56$, $\theta_1 = 130°$.

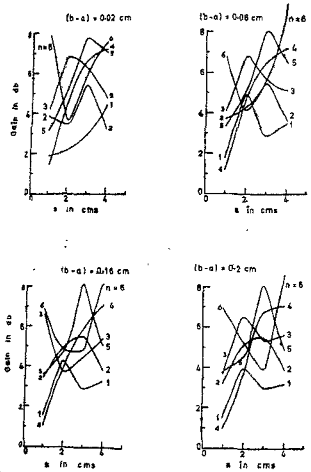

FIG. 13. Variation of gain with the inner radius 'a'. f $= 9 \cdot 375$ GHz, $\varepsilon_r = 2 \cdot 56$, $\theta_1 = 130°$.

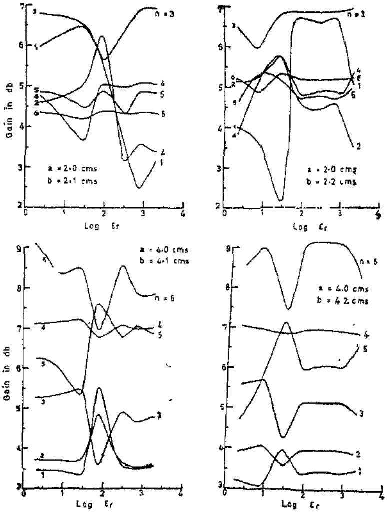

FIG. 14. Variation of the gain with ε_r the relative permittivity of the coating material. f =9 375 GHz, $\varepsilon_r = 2 \cdot 56$, $\theta_1 = 130°$.

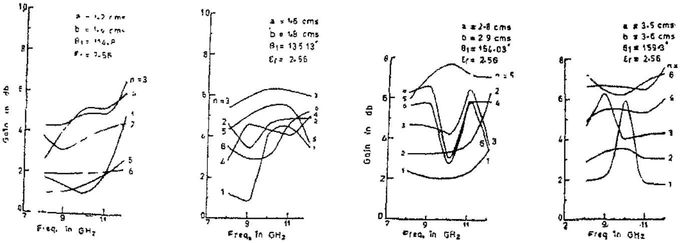

FIG. 15. Variation of gain with the frequency of excitation.

The variation of the gain with $(b-a)$ and a for the case of equatorial excitation is shown in Figs. 17 and 18 for the TM_{01}, TM_{03} and TM_{05} modes.

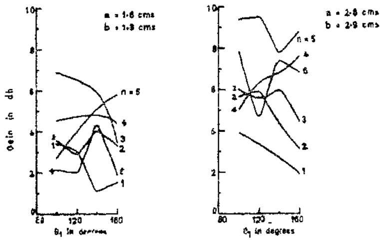

FIG. 16. Variation of gain with angle of excitation θ_1. f = 9·375 GHz, $\varepsilon_r = 2{\cdot}56$.

From the theoretical analysis of the gain of the truncated dielectric-coated conducting spherical antenna it may be concluded that the gain is affected significantly by the various structure parameters mentioned above.

6. Experimental verification

6.1. *Radiation pattern and gain characteristics*

The radiation patterns and gain characteristics have been measured at the frequency 9·375 GHz at the out-door microwave laboratory. The experiments have also been conducted in the range 8·0 to 12·0 GHz at the antenna test range at LRDE, Bangalore, and at the microwave anechoic chamber at DLRL, Hyderabad.

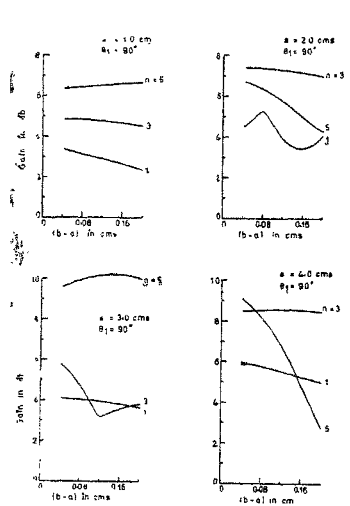

FIG. 17. Variation of gain with coating thickness for equatorial excitation. f = 9·375 GHz, $\varepsilon_r = 2{\cdot}56$.

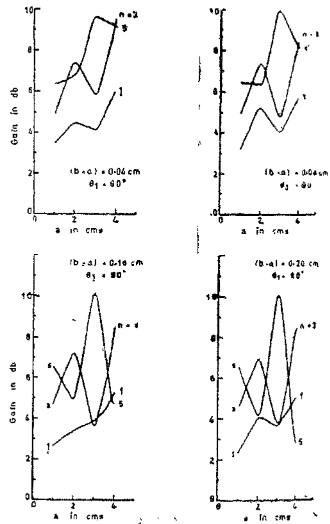

FIG. 18. Variation of gain with the inner radius 'a' for equatorial excitation. f = 9·375 GHz, $\varepsilon_r = 2{\cdot}56$.

The observed radiation patterns are shown in Figs. 19 *a*, *b*, *c* along with the theoretical patterns. The patterns have been normalized w.r.t. the maximum of the radiated power.

The theoretical radiation patterns have been shown only for the TM_{05} on TM_{06} mode. It is seen that there is good agreement between theory and experiment for these modes. The comparison between theory and experiment shows that:

(1) the position of the main lobe for all the structures studied experimentally compares well with theory.

(2) there is good agreement between the beam width of the main lobe for the experimental and calculated patterns.

(3) the number of side lobes obtained experimentally differs in a few cases from that obtained theoretically. The positions of the side lobes agree fairly well with experiment and theory.

(4) the amplitudes of the side lobes obtained theoretically and experimentally show fair agreement.

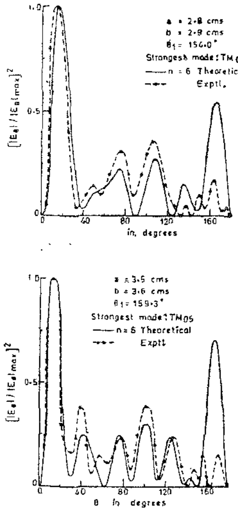

G. 19 *a*. Theoretical and experimental normalized diation patterns. f = 9·375 GHz, $\varepsilon_r = 2\cdot56$.

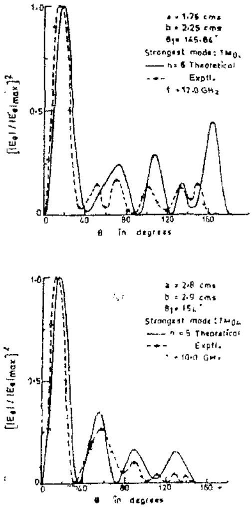

FIG. 19 *b*. Theoretical and experimental normalized radiation patterns. $\varepsilon_r = 2\cdot56$.

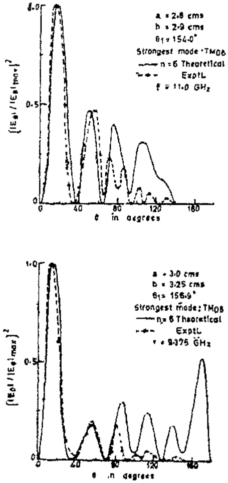

FIG. 19 *c*. Theoretical and experimental normalized radiation patterns. $\varepsilon_r = 2 \cdot 56$.

(5) The positions of the minima and their intensities in the experimental patterns compare well with the calculated patterns.

An attempt has been made to determine the effect of the other modes combined with the TM_{05} and TM_{06} modes on the radiation pattern. The radiation patterns for the combined modes, the TM_{06} mode and the experimental pattern at a frequency $f = 9 \cdot 375$ GHz are shown in Fig. 20. There is no agreement between the experimental and theoretical pattern for the combined modes. The position of the main lobe and the main lobe beam width for the combined mode and the individual TM_{05} and TM_{06} modes along with the experimental results is given in Tables III and IV for the frequency of excitation = 9·375 GHz. In Table III it is seen that there is considerable divergence between theory and experiment in each of the cases, whereas there is close agreement between theory and experiment for the individual TM_{05} and TM_{06} modes as is evident from Table IV.

Table III

Comparison of the theoretical position of the main lobe and the main lobe beam width for six modes combined with experiment

$f = 9 \cdot 375$ GHz

a cm	b cm	θ_1 degs	Position of the main lobe in degrees		Main lobe beam width in degrees	
			Theory	Expt	Theory	Expt
1·6	1·8	135·1	30	23	40	20
1·75	2·25	145·6	26	20	27	20
2·8	2·9	154·0	20	14	19	18
3·0	3·25	156·9	20	14	20	13
3·5	3·6	159·3	18	12	19	12

The results of the gain obtained experimentally are given in Table V along with the theoretical results for various structures. Table VI gives the experimental and theoretical values at different frequencies of excitation. It is seen that the experimental values agree with the theoretical results for the TM_{05} and TM_{06} modes. The values of the gain obtained experimentally and those obtained theoretically for the summation of the first six modes at a frequency of 9·375 GHz (not given here) differ considerably.

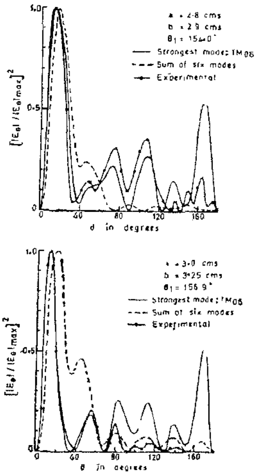

FIG. 20. The normalized radiation pattern for the strongest mode and the sum of first six modes with the experimental pattern. f = 9·375 GHz, ε_r=2·56.

7. Conclusions

The theoretical and experimental investigations on the radiation characteristics of the truncated dielectric-coated conducting spherical antenna lead to the following conclusions:

(1) The structure excited in the symmetric TM mode in the frequency range 8·0 to 12·0 GHz is characterized by a radiation pattern having a null on the axis ($\theta = 0°$) and two major lobes situated symmetrically with respect to the axis, and a few side lobes.

Table IV

Comparison of the theoretical position of the main lobe and the main lobe beam width for the individual modes with experiment

f = 9·375 GHz

a cm	b cm	θ_1 degs	Mode	Position of the main lobe in degrees		Main lobe width in degrees	
				Theory	Expt	Theory	Expt
1·6	1·8	135·1	TM_{05}	26	23	44	20
1·75	2·25	145·6	TM_{05}	18	20	25	20
2·8	2·9	154·0	TM_{06}	16	14	19	18
3·0	3·25	156·9	TM_{06}	12	14	14	13
3·5	3·6	159·3	TM_{06}	12	12	13	12

Table V

Comparison of the theoretical and experimental values of gain

a cm	b cm	θ_1 degs	Theoretical gain in db for mode						Experimental value of gain in *db*
			TM_{01}	TM_{02}	TM_{03}	TM_{04}	TM_{05}	TM_{06}	
1·6	1·8	135·1	1·77	3·76	6·38	4·33	5·41	2·94	5·05
1·75	2·25	145·6	2·26	3·74	4·44	6·38	4·67	3·28	4·75
2·8	2·9	154·0	2·26	3·09	4·77	7·06	6·82	7·84	7·55
3·0	3·25	156·9	2·19	3·55	5·90	5·78	6·76	5·45	6·55
3·5	3·6	159·3	2·34	5·34	3·80	5·42	6·64	5·84	6·05

Table VI

Comparison of the theoretical and experimental values of gain at different frequencies

$a = 2 \cdot 8$ cm, $b = 2 \cdot 9$ cm, $\theta_1 = 154°$, $\epsilon_r = 2 \cdot 56$.

Frequency in GHz	Theoretical gain in db for mode						Experimental gain in db
	TM_{01}	TM_{02}	TM_{03}	TM_{04}	TM_{05}	TM_{06}	
8·0	2·44	3·29	4·68	6·31	5·99	5·68	5·60
9·0	2·21	3·30	4·60	6·59	7·10	5·76	6·80
10·0	2·20	3·39	4·28	3·06	7·76	2·84	6·30
11·0	2·47	3·81	6·46	5·84	7·29	5·93	5·80

(2) The radiation characteristics of the antenna are sensitive to the various structure parameters such as the inner radius, coating thickness, angle of excitation, etc., and hence can be controlled by a suitable choice of the parameters.

(3) There is agreement between the experimental and theoretical radiation characteristics for the TM_{05} and TM_{06} modes.

(4) The antenna has a low gain.

8. Acknowledgements

The authors are grateful to Dr. S. Dhawan, Director, Indian Institute of Science, for providing facilities for the work and to the Council of Scientific and Industrial Research for the sanction of a scheme on this subject. They are also grateful to the authorities of LRDE, Bangalore, and DLRL, Hyderabad, for allowing part of the experimental work to be conducted at their establishments.

References

1. TING, C. I. — Infinite cylindrical dielectric-coated antenna, *Radio Science*, 1967, **2**, 325–335.
2. CHATTERJEE, R. AND CHANDRAKALADHAR RAO, T. — Dielectric-coated circular cylindrical metal antennas excited in the TM symmetric mode at microwave frequencies, *Jour. Radio Space Physics*, 1974, **3**, 167–171.
3. CHATTERJEE, R. AND CHANDRAKALADHAR RAO, T. — Circular cylindrical dielectric-coated metal rod excited in the symmetric TM_{01} mode. Part II : Radiation characteristics, *Jour. Ind. Inst. Sc.*, 1973, **55** (4), Pp 232–254.
4. CHATTERJEE, R. AND VIRUPAKSHA, S. — Radiation from a finite-length dielectric-coated spherically-tipped conducting cone antenna excited in the symmetric TM mode at microwave frequencies, *IEE—IERE Proceedings, India*, 1975, **13** (6), 218–229.
5. CHATTERJEE, R. AND VEDAVATHY, T. S. — Dielectric-coated spherically-tipped conducting cone antenna excited in the unsymmetric hybrid mode at microwave frequencies, *Jour. Ind. Inst. Sc.*, 1975, **57** (11), Pp 399–425.
6. YEH, C. W. H. — On the dielectric-coated prolate spheroidal antenna, *Jour. Math. Phys.*, 1963, **42**, 68.
7. NEELAKANTASWAMY, P. S. AND BANERJEE, D. K. — Corrugated spherical antenna, *Electronics Letters*, Nov. 2, 1972, **8** (22), 534–536.
8. CHATTERJEE, R., KESHAVAMURTHY, T. L. AND VEDAVATHY, T. S. — Dielectric-coated spherical metal antennas excited in the unsymmetric hybrid mode at microwave frquencies, *J. I.E.T.E.*, India, 1974, **20** (8), 386.
9. CHATTERJEE, R., VEDAVATHY, T. S., WAHID, P. AND NAGESH, B. K. — Dielectric-coated metal spherical antennas excited in the symmetric TM mode at microwave frequencies, *IEE-IERE Proceedings, India*, 1974, **12** (3), p. 888.
10. CHATTERJEE, R. AND WAHID, P. — Truncated dielectric-coated conducting sphere excited in the TM symmetric mode as an antenna, *IEE-IERE Proceedings, India*, 1977, **15** (5), 195.
11. WAHID, P. AND CHATTERJEE, R. — The dielectric-coated conducting sphere—modal and near-field characteristics, *Jour. Ind. Inst. Sc.*, 1979, **61** (A), 105–125.
12. CHATTERJEE, R. — Electromagnetic boundary value problem of the dielectric-coated conducting sphere excited by delta-function electric and magnetic sources, *Jour. Ind. Inst. Sc.*, 1974, **56** (3), 107–127.

Appendix

Table A

The number, position and relative intensity of the side lobes with respect to the main lobe for the dielectric-coated conducting spherical antenna

$(b-a) = 0\cdot 1$ cm, $\theta_1 = 140°$, $f = 9\cdot 375$ GHz, $\epsilon_r = 2\cdot 56$.

a cm	b cm	No. of side lobes for mode					
		TM$_{01}$	TM$_{02}$	TM$_{03}$	TM$_{04}$	TM$_{05}$	TM$_{06}$
1·0	1·1	..	1	2	1	..	..
1·5	1·6	..	1	2	3	2	..
2·0	2·1	..	1	2	3	3	3
2·5	2·6	..	1	2	3	3	4
3·0	3·1	..	1	3	3	3	4
3·5	3·6	1	2	3	3	4	4
4·0	4·1	1	2	3	3	4	5
		Position (in degs.) and relative intensity (in db) of the side lobes (in brackets) for mode					
1·0	1·1	..	41 (−1·08)	29 (−1·87) 151 (−0·30)	49 (−1·05)	..	..
1·5	1·6	..	41 (−1·77)	29 (−2·85) 87 (−3·67)	25 (−1·48) 57 (−0·74) 159 (−2·71)	39 (−1·44) 137 (−1·81)	..
2·0	2·1	..	37 (−2·46)	27 (−3·73) 89 (−5·36)	25 (−1·96) 55 (−4·01) 111 (−2·55)	87 (−1·57) 129 (−3·41) 161 (−3·92)	23 (−1·11) 73 (−1·01) 157 (−2·82)
2·5	2·6	..	33 (−3·03)	25 (−4·28) 93 (−5·78)	23 (−4·02) 55 (−6·01) 111 (−5·12)	85 (−3·92) 125 (−2·64) 161 (−1·47)	71 (−4·95) 103 (−4·33) 135 (−7·07)
3·0	3·1	..	29 (−3·39)	23 (−4·43) 65 (−9·69) 95 (−4·80)	19 (−5·35) 55 (−6·72) 113 (−6·29)	23 (−1·61) 85 (−2·52) 123 (−3·64)	71 (−8·22) 103 (−6·86) 137 (−5·88) 165 (−3·52)
3·5	3·6	27 (−7·31)	27 (−7·33) 63 (−2·56)	21 (−3·87) 67 (−8·84) 95 (−3·16)	17 (−5·97) 55 (−7·03) 115 (−6·11)	21 (−4·07) 47 (−6·97) 87 (−7·65) 123 (−5·53)	43 (−11·18) 71 (−9·42) 103 (−8·13) 133 (−5·47)
4·0	4·1	27 (−7·31)	25 (−4·49) 57 (−2·09)	17 (−2·72) 49 (−7·43) 95 (−1·76)	13 (−5·85) 67 (−6·67) 113 (−5·19)	25 (−6·56) 49 (−6·17) 89 (−8·13) 123 (−6·72)	41 (−8·86) 73 (−10·6) 103 (−8·17) 133 (−5·59)